Extension of a Martian general circulation model to thermospheric altitudes: UV heating and photochemical models

F. González-Galindo,[1] M. A. López-Valverde,[1] M. Angelats i Coll,[2,3] and F. Forget[2]

Received 25 June 2004; revised 14 June 2005; accepted 24 June 2005; published 22 September 2005.

[1] A fast method to incorporate the UV heating and the photochemistry of the neutral upper atmosphere of Mars into general circulation models (GCMs) is presented. On the basis of more detailed one-dimensional (1-D) models, the scheme we propose makes use of a division of the UV spectrum in 36 subintervals of 20 nm average width. Photoabsorption coefficients are computed allowing for overlapping and are tabulated as a function of suitable column abundances. The photochemistry proposed includes 12 compounds and uses the approximation of photochemical equilibrium for the three fastest species, OH, O(^{1}D), and HO_2. The behavior of the fast scheme is shown against detailed 1-D calculations. The resulting acceleration is about a factor 200 in the UV heating, while in the photochemistry it is about a factor 100 at 120 km and much larger below. The proposed scheme has already been implemented into the GCM developed at the Laboratoire de Météorologie Dynamique-CNRS in Paris (LMD), which therefore becomes the first single Martian GCM to cover the whole range of altitudes from the planet surface to the upper thermosphere. We present typical results of the Martian thermosphere obtained with the present scheme and the LMD-GCM, in order to illustrate its behavior and stability. In particular, we show the sensitivity of the Martian upper atmosphere's thermal structure to the local photochemistry. Comparisons with previous models are also presented, as first steps in an ongoing validation study, necessarily extensive for this kind of GCM, which will include more detailed comparisons with recent and future data from space missions.

Citation: González-Galindo, F., M. A. López-Valverde, M. Angelats i Coll, and F. Forget (2005), Extension of a Martian general circulation model to thermospheric altitudes: UV heating and photochemical models, *J. Geophys. Res.*, *110*, E09008, doi:10.1029/2004JE002312.

1. Introduction

[2] New modeling efforts and new data from spacecraft instrumentation are two relevant topics of the renovated interest on the upper atmosphere of Mars. On the side of the theoretical modeling and simulation, a number of general circulation models (GCM) are under development with the purpose of studying the behavior of this region and its coupling with lower altitudes. GCMs have been revealed as powerful tools to study atmospheric processes and their interactions in planetary atmospheres, to simulate temperature, pressure, and wind fields, as well as to extract the most information out of diverse and disperse data sets. The normally huge number of calculations involved in GCM simulations makes it necessary to use efficient numerical algorithms and approximations to implement the diverse physical processes required, like radiative transfer, whose detailed treatment would be very CPU time consuming [*Holton*, 1992; *Hourdin et al.*, 1996].

[3] Some GCMs have been developed in the last decades for the study of the Martian atmosphere, like the NASA/AMES "MGCM" [*Pollack et al.*, 1990; *Haberle et al.*, 1993, 1999], the thermospheric "MTGCM" originally developed at the National Center for Atmospheric Research [*Bougher et al.*, 1990, 1999, 2000], the GFDL Mars-GCM [*Wilson and Hamilton*, 1996] and that developed by a British and French consortium "LMD/AOPP MGCM" [*Hourdin et al.*, 1993; *Forget et al.*, 1999]). However, with the exception of the MTGCM, all these efforts have been confined to study diverse problems in the lowest layers of the Martian atmosphere due to the scarcity of data in the Martian mesosphere and thermosphere. For example, the NASA/AMES "MGCM" has been used to forecast the meteorological environment of the Mars Pathfinder landing site [*Haberle et al.*, 1997], to study the CO_2 seasonal cycle [*Smith et al.*, 1999], or to study the temperature profiles measured by the Mars Global Surveyor (MGS) [*Joshi et al.*, 2000]. The GFDL Mars-GCM has been employed to study aspects like thermal tides [*Hinson*

[1] Instituto de Astrofísica de Andalucía, CSIC, Granada, Spain.
[2] Laboratoire de Météorologie Dynamique, CNRS, Paris, France.
[3] Now at Department of Earth and Space Sciences, University of California, Los Angeles, California, USA.

0148-0227/05/2004JE002312$09.00

and Wilson, 2004], the water cycle [*Richardson and Wilson*, 2002], or the dust cycle [*Basu et al.*, 2004]. The LMD/AOPP MGCM has allowed to study the annual surface pressure cycle [*Hourdin et al.*, 1993], to simulate the CO_2 snowfall [*Forget et al.*, 1998], or to create a database of the Martian climate useful for mission planing and design [*Lewis et al.*, 1999]. Recently, it has also been used in the analysis of thermospheric data from the Mars Global Surveyor's accelerometer [*Angelats i Coll et al.*, 2003a, 2003b, 2004]. Regarding the only Mars thermospheric GCM until recently, the MTGCM, this has been a world reference for studies of the upper Martian atmosphere and has been used in a number of comparative studies of the terrestrial planet thermospheres [*Bougher and Roble*, 1991; *Bougher et al.*, 1999, 2000], or in analyzing the electron density profiles measured by MGS [*Bougher et al.*, 2001], to mention a few applications. Recently, this model has been used in conjunction with the NASA/AMES MGCM [*Bougher et al.*, 2004]. The models are coupled at the 1.32 μbar level, with the key fields being passed upward from the NASA/AMES MGCM to the MTGCM. This coupling has proven effective for capturing migrating and nonmigrating tides [*Bougher et al.*, 2004]. However, no downward coupling from the MTGCM to the NASA/AMES MGCM is used at the moment.

[4] In order to be useful in the design of aerobraking maneuvers at thermospheric altitudes and to interpret new observations (e.g., from SPICAM on Mars Express), the upper limit of the LMD-GCM has been recently raised, thus becoming the first GCM covering the whole Martian atmosphere [*Angelats i Coll et al.*, 2005]. For this purpose, new parameterizations of the physical processes relevant to the upper Martian atmosphere were included. In particular, the UV heating, which is the main energy input of the Martian upper atmosphere above about 120 km [*Fox and Dalgarno*, 1979; *Bougher et al.*, 1999], and the appropriate photochemistry. This was the main motivation of the fast scheme that we present and propose here for its implementation in Martian GCM models that cover the upper atmosphere. The idea of extending a GCM from the ground to the upper Martian atmosphere is under active investigation also in other laboratories [*Crowley et al.*, 2003; *Ridley et al.*, 2004; *Mouden and McConnell*, 2005].

[5] Both UV and photochemical modules of our fast scheme use as a reference more detailed methods included in the one-dimensional (1-D) nonstationary model of the Martian upper atmosphere currently under development at the Instituto de Astrofísica de Andalucía, based on a previous 1-D convective and radiative-equilibrium time-marching model, with detailed treatment of non−local thermodynamic equilibrium [*López-Valverde et al.*, 1998, 2000]. Improvements now incorporated into the 1-D model include a UV heating model, a chemical code of the neutral atmosphere, and a number of transport schemes. We will present here how these more detailed models have been simplified, including approximations and parameterizations, in order to reduce their CPU time consumption and to make them suitable to be implemented in a Martian GCM.

[6] In this paper, the UV heating "detailed" model is first briefly described in section 2, as it will be useful in section 3 to present the fast scheme proposed here. Description of the photochemical scheme is included in section 4. Guidelines to implement the fast schemes into a generic Martian GCM are given in section 5. Details of their implementation and behavior into the LMD GCM including some results like the effect of the photochemistry and of the solar cycle on the thermospheric temperatures are shown in section 6.

2. Reference UV Heating Calculations

[7] The reference calculations of UV heating in the upper atmosphere of Mars have been performed with a 1-D model, which solves the usual monochromatic radiative transfer equation for the absorption of solar flux in an atmosphere [*Houghton*, 1977]. It uses a detailed raytracing approach to obtain the optical depth τ for solar zenith angles larger than 85 degrees and the Chapman function for lower angles. Once τ is evaluated and given the solar flux at the top of the atmosphere, the monochromatic photoabsorption coefficient, j_i, for each constituent, i, is calculated from the top of the atmosphere downward following a usual onion-peeling method (see, for example, *Brasseur and Solomon* [1986]). This coefficient is a key magnitude in the study of photochemical processes. Finally, the UV atmospheric heating rate Q_{UV} is calculated at each altitude, z, by a spectral integration:

$$Q_{UV}(z) = \eta(z)\frac{hc}{\lambda}\int_{\lambda_{\min}}^{\lambda_{\max}} \sum_i j_{i,\lambda}(z) n_i(z) \mathrm{d}\lambda, \qquad (1)$$

where $n_i(z)$ is the number density of this compound and η is the UV + EUV heating efficiency, i.e., the fraction of the initial absorption that is finally thermalized. Its detailed evaluation requires a complex analysis of radiation-matter interactions not free from a number of important uncertainties [*Fox and Dalgarno*, 1979, 1981]. In this work we use the standard value $\eta = 0.22$, constant with altitude, following the detailed model by *Fox* [1988].

[8] The previous equation is solved after discretization to a fine grid in altitude from the surface up to 250 km and with sufficiently high spectral resolution. We compute the absorption by CO_2, O_2, O, H_2, H_2O, H_2O_2, and O_3 in the 0.1−800.0 nm spectral range.

[9] Input data needed by the model include the cross sections for absorption of the different species and the solar flux at top of the atmosphere (TOA) and also some initial states given by diverse atmospheric profiles of temperature, pressure, and abundances of those compounds.

2.1. Input Data

[10] The absorption cross sections were taken from several sources [*Brasseur and Solomon*, 1986; *Atreya and Gu*, 1994; *Torr et al.*, 1979; *Yoshino et al.*, 1988, 1992, 1996; *Roble and Emery*, 1983; *Yung and DeMore*, 1999; *Banks and Kockarts*, 1973, *Parkinson et al.*, 2003, *Parkinson and Yoshino*, 2003].

[11] Let us recall that the temperature dependence of the CO_2 cross section between 118.7 and 210.0 nm is important for the solar absorption in the middle and lower Martian atmosphere [*Anbar et al.*, 1993], affecting not only the photodissociation rate of CO_2 but also the dissociation of H_2O and O_2, lessening the problem of the stability of CO_2 [*Nair et al.*, 1994]. We used the dependence given by *Anbar et al.* [1993] and the data from *Yoshino et al.* [1996]: a linear

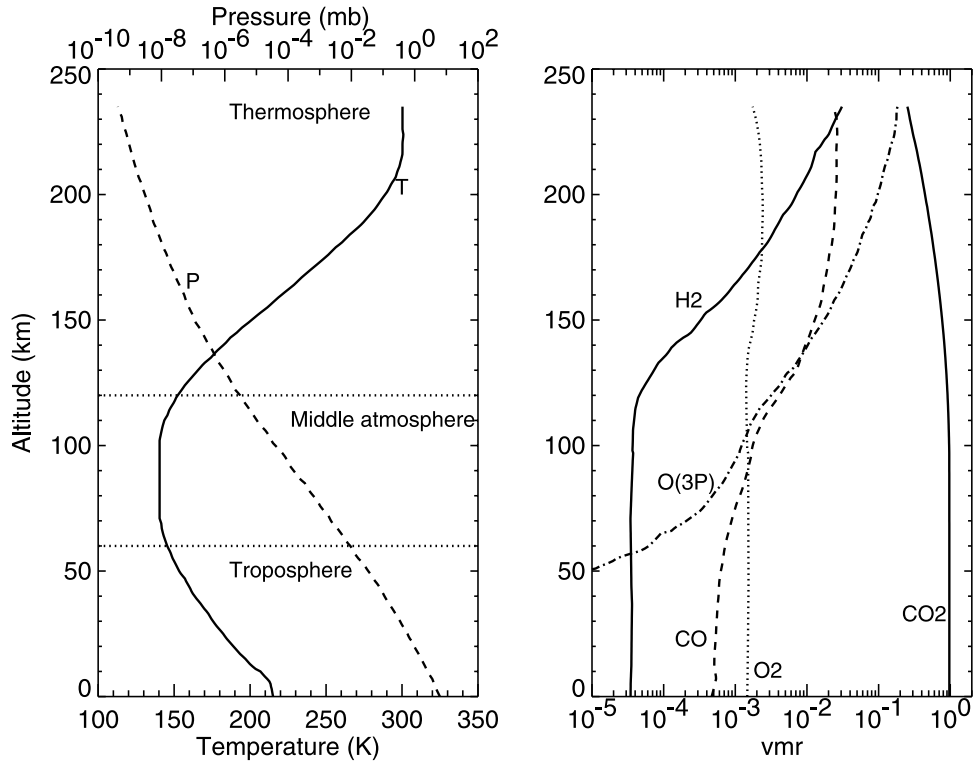

Figure 1. (left) Temperature (solid) and pressure (dashed) and (right) relative abundances of some key compounds for the reference atmosphere. See text for more details.

variation of the monochromatic cross section between 195 K and 295 K. Below 195K and above 295K no temperature dependence is considered, as in the nominal model of *Nair et al.* [1994]. This last assumption may affect the photoabsorption rates in the lower atmosphere, as discussed by *Nair et al.* [1994] (see, for example, their Figure 16). The cross section for Rayleigh scattering for CO_2 is also included, following *Atreya and Gu* [1994].

[12] The solar flux at TOA was taken from the "SOLAR2000" database [*Tobiska et al.*, 2000] for solar maximum ($F_{10.7}$ = 224.1), medium ($F_{10.7}$ = 118.3), and minimum conditions ($F_{10.7}$ = 73.8), and scaled to the appropriate Sun-Mars distance. The original, high resolution data for the solar flux and cross sections have been averaged to a 1 nm spectral regular grid for the calculations in this work; a sample of calculations performed for higher spectral resolution did not show differences.

[13] Calculations for this work were performed for a temperature/density reference atmosphere appropriate for medium solar activity conditions, shown in Figure 1. This and the gases abundances profiles were taken from *Nair et al.* [1994], and the surface pressure was set to 6.4 mbar. This 1-D model can handle any altitude grid; for this work, a 1-km regular grid was used.

2.2. Selected Results

[14] Typical results of atmospheric heating rates due to the different constituents are shown in Figure 2. The largest contribution obviously comes from the major constituent of the Mars atmosphere, CO_2, which is responsible for a maximum heating rate of about 500 K/day around 150 km altitude, for moderate conditions of solar activity. Even in the upper layers of the atmosphere, where O is as abundant as CO_2, the latter is the dominant heater, showing that CO_2 is more efficient heating the atmosphere than O, because it absorbs radiation in a wider spectral range.

[15] Comparisons with nominal results from other models of UV solar heating of the Martian upper atmosphere were performed within an intercomparison campaign carried out recently [*López-Valverde et al.*, 2003]. While an excellent agreement was obtained with the photoabsorption coefficients for CO_2 and O_2 of the UV absorption model by the Service d'Aeronomie [*Lefevre et al.*, 2004], significant differences with the O_2 photoabsorption coefficients of the MTGCM [*Bougher et al.*, 1999] were obtained. These are probably due to the use of different absorption cross sections in the Lyman α region and at wavelengths higher than 190 nm.

3. UV Heating Fast Scheme

[16] An approximation to the atmospheric optical path is at the core of our scheme. The optical depth depends both on the abundances of the different compounds and on their cross sections. If the monochromatic cross sections of each species i are not dependent on temperature or pressure, which is an approximation appropriate for the upper atmosphere, then the optical depth τ_λ can be expressed

$$\tau_\lambda(z) = \frac{1}{\mu}\sum_{i=1}^{N_{gases}} \sigma_{i,\lambda} \int_z^{z_{TOA}} n_i(z')dz' \qquad (2)$$

and the only variation with altitude is due to the column amounts of the different absorbers. This idea, used previously in UV heating calculations for the terrestrial atmosphere (see, for example, *Zhao and Turco* [1997, and

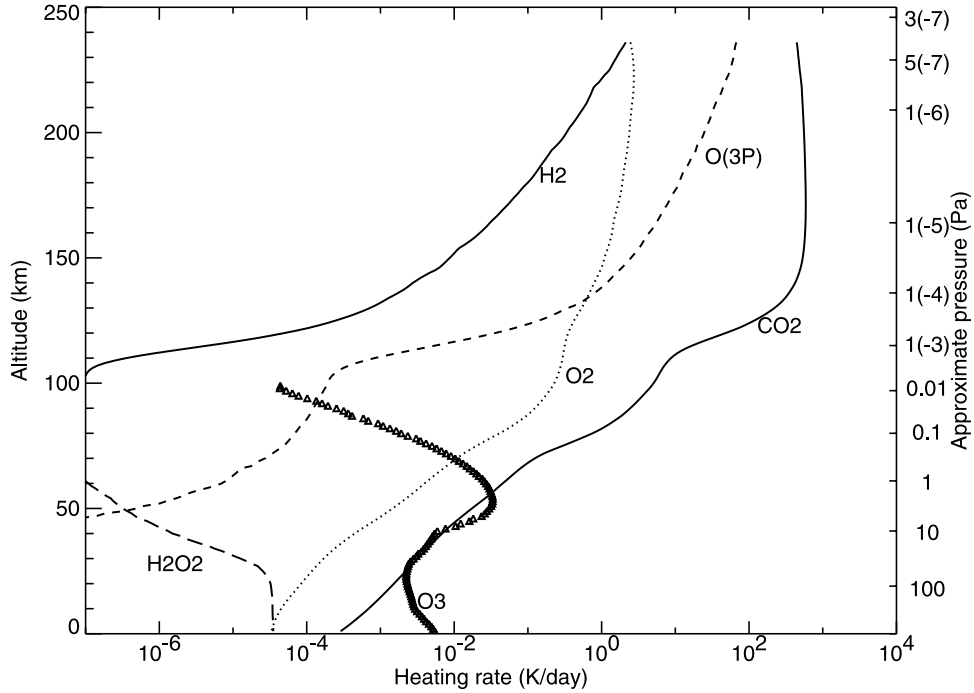

Figure 2. Profile of the total heating rate for zenith conditions, with contributions from different species, for solar medium activity.

references therein] and *Chipperfield* [1999]), is novel in calculations for the Martian upper atmosphere. We considered the constituents CO_2, O_2, O, H_2, H_2O, H_2O_2, and O_3. As it is customary, we divided the spectral range in subintervals or windows of varying widths. Our criteria was not only to minimize the spectral variation of the nominal solar flux and the absorption cross sections (or at least to obtain a linear variation within each subinterval) but also to have similar variations of the solar flux during the solar cycle at all frequencies within each subinterval. This procedure resulted in a total of 36 windows with a typical width of about 20 nm, which are listed in Table 1. The species with significant absorption in each subinterval are also listed. In each subinterval, and for our reference atmosphere, we computed the integrated photoabsorption coefficient for each absorber with the detailed 1-D model and tabulated it as a function of the total column amount of all the constituents with absorption in that interval. Then, in order to obtain the photoabsorption coefficients for a given subinterval and for a particular atmospheric profile, one only has to interpolate to the actual total column amount appropriate for this subinterval of the new atmosphere. This magnitude either is readily available or should be easily obtained at each altitude in any GCM model.

3.1. Temperature Dependence

[17] We wanted to incorporate a suitable correction term in some subintervals of this scheme in order to handle the temperature dependence of the CO_2 cross section. Let us suppose that the temperature variation of the cross section of CO_2, for which let us use index $i = 1$ in equation (2), is given, between 195 K and 295 K by a linear relation of the form:

$$\sigma_{1,\lambda}(T) = \sigma_{1,\lambda}(T_0)\big(1 + \alpha_{1,\lambda}(T - T_0)\big).$$

Below 195 K and above 295 K no temperature dependence is considered. Following *Anbar et al.* [1993] and using $T_0 = 195$ K, we can express, without further approximations,

$$\sigma_{1,\lambda}(T) = \sigma_{1,\lambda}(T_0) + \frac{\sigma_{1,\lambda}(295) - \sigma_{1,\lambda}(T_0)}{295 - T_0}(T - T_0)$$

from where we obtain

$$\alpha_{1,\lambda} = \frac{\frac{\sigma_{1,\lambda}(295)}{\sigma_{1,\lambda}(T_0)} - 1}{295 - T_0}.$$

Therefore it is possible to know the proportionality factor $\alpha_{1,\lambda}$ as a function of the cross section at two temperatures, $\sigma_{1,\lambda}(295)$ and $\sigma_{1,\lambda}(195)$.

[18] The effect of the temperature variation of CO_2 cross section over the optical depth (by all the atmospheric constituents) is

$$\begin{aligned}\tau_\lambda(T) &= \sum_{i=1}^{N_{gases}} \int_z^{z_{TOA}} \sigma_{i,\lambda}(T(z)) n_i(z) \mathrm{d}z_i \\ &= \tau_\lambda(T_0) + \sigma_{1,\lambda}(T_0)\alpha_{1,\lambda} \int_z^{z_{TOA}} \Delta T n_1(z) \mathrm{d}z.\end{aligned}$$

[19] Thus a correction term to the optical depth appears that will affect the absorption of any other constituent, not only CO_2. The photoabsorption coefficient of CO_2 can now be computed straightforwardly by

$$\begin{aligned}j_{1,\lambda}(T(z)) = \; & j_{1,\lambda}(T_0) \\ & \cdot \exp\left(-\sigma_{1,\lambda}(T_0)\alpha_{1,\lambda} \int_z^{z_{TOA}} \Delta T n_1(z) \mathrm{d}z\right) \\ & \cdot \big(1 + \alpha_{1,\lambda}\Delta T\big). \end{aligned} \quad (3)$$

Table 1. Subdivision of Spectral Range in Intervals[a]

No.	Interval, nm	Δλ, nm	Absorbers	c1	p1	c2	p2
1	0.1–5.0	4.9	O_2,$O(^3P)$, H_2	71.663	−0.03564	66.341	−0.03277
2	5.0–10.4	5.3	CO_2,O_2, $O(^3P)$, H_2	44.377	−0.02201	40.919	−0.02006
3	10.4–16.5	6.1	"	44.414	−0.02201	40.945	−0.02007
4	16.5–29.4	12.8	"	51.521	−0.02555	51.255	−0.02519
5	29.4–31.5	2.0	"	46.031	−0.02284	46.063	−0.02259
6	31.5–38.5	6.9	"	49.024	−0.02434	46.236	−0.02271
7	38.5–50.4	11.8	"	45.014	−0.02233	42.641	−0.02091
8	50.4–51.4	0.4	"	21.874	−0.01088	20.451	−0.00977
9	51.4–53.4	1.9	"	20.110	−0.00988	22.8487	−0.01097
10	53.4–58.4	4.9	"	5.054	−0.00249	6.114	−0.00256
11	58.4–59.4	0.9	"	37.625	−0.01864	38.929	−0.01899
12	59.4–63.5	4.0	"	9.400	−0.00455	9.676	−0.00434
13	63.5–70.5	6.9	"	7.753	−0.00381	8.8459	−0.00393
14	70.5–75.5	4.9	"	0.	0.	0.	0.
15	75.5–80.5	4.9	"	1.501	−0.00065	11.051	−0.00501
16	80.5–90.8	10.2	CO_2, O_2, $O(^3P)$	7.619	−0.00374	8.748	−0.00388
17	90.8–96.5	5.6	CO_2, O_2	11.169	−0.00548	12.359	−0.00568
18	96.5–98.5	1.9	"	11.918	−0.00585	13.1178	−0.00606
19	98.5–99.5	0.9	"	8.94	−0.00439	10.092	−0.00455
20	99.5–100.5	0.9	"	8.89	−0.00436	10.032	−0.00452
21	100.5–101.5	0.9	"	1.098	−0.00054	2.113	−0.00056
22	101.5–102.5	0.9	"	33.462	−0.01658	34.418	−0.01675
23	102.5–106.3	3.7	"	6.509	−0.00320	7.617	−0.00331
24	106.3–119.5	13.1	"	4.871	−0.00239	5.960	−0.00248
25	119.5–123.5	3.9	CO_2, O_2, H_2O, H_2O_2	-	-	-	-
26	123.5–129.6	6.0	"	-	-	-	-
27	129.6–134.5	4.8	"	-	-	-	-
28	134.5–158.5	23.9	"	-	-	-	-
29	158.6–167.0	8.4	"	-	-	-	-
30	167.0–175.6	8.5	"	-	-	-	-
31	175.6–202.5	26.8	"	-	-	-	-
32	202.5–210.0	7.5	CO_2, H_2O_2	-	-	-	-
33	210.0–230.9	20.8	H_2O_2, O_2	-	-	-	-
34	230.9–240.0	9.0	H_2O_2, O_2, O_3	-	-	-	-
35	240.0–337.7	97.6	H_2O_2, O_3	-	-	-	-
36	337.7–800.0	462.2	O_3	-	-	-	-

[a]Δλ is the width of the interval, in nm. c_1, p_1, c_2, and p_2 are the parameters for the solar flux variation as stated in equation (5) (see text for more details).

[20] As we see, we have two correction terms, one due directly to the variation of the cross section of CO_2 ($(1 + \alpha_{1,\lambda}\Delta T)$) and another one due to the variation of the transmittance of the atmosphere ($\exp(-\sigma_{1,\lambda}(T_0)\alpha_{1,\lambda}\int_z^{z_{TOA}} \Delta T n_1(z)\mathrm{d}z)$).

[21] For the rest of the constituents, there is only one correction term for the atmospheric transmittance, as mentioned above:

$$j_{i,\lambda}(T(z)) = j_{i,\lambda}(T_0) \cdot \exp\left(-\sigma_{1,\lambda}(T_0)\alpha_\lambda \int_z^{z_{TOA}} \Delta T n_1(z)\mathrm{d}z\right) \; (i \neq 1) \quad (4)$$

[22] Given the proportionality factors $\alpha_{1,\lambda}$ for each subinterval and the temperature T_0 of the atmosphere employed to build the tabulation, these correction terms can be easily computed in a GCM once the column amounts are already known, which we assumed before.

3.2. Solar Flux Variability

[23] It is desirable for long-term runs of a GCM to implement the solar cycle variation into the present scheme. We show here how our scheme allows to take into account such variation, or any other known/predicted solar flux variability.

[24] A common way of modeling the solar variability is by using the $F_{10.7}$ index as a proxy model [*Lean*, 1987]. Although this is a reliable indicator of the general level of solar activity, its correlation with the solar UV flux in narrow wavelength regions is less reliable [*Donnelly et al.*, 1986]. This is because the 10.7 cm flux originates predominantly only from the upper chromosphere and lower corona, while the UV emissions originate from a wider range of heights in the solar atmosphere extending from the lower chromosphere to the corona. Since these areas can be very affected by different physical processes, it is not surprising that the UV flux does not correlate well with the 10.7 cm flux [*Heroux and Hinteregger*, 1985].

[25] Taking this evidence into account, we decided to follow a different strategy, based on the work by *Dyominov and Zadorozhny* [2001] and on the observation of the complete solar cycle 22nd and the incomplete 23rd (1985–2001).

[26] We took the solar flux time curve in each one of the 36 wavelength intervals and fitted a sinusoidal function with four free parameters, of the form:

$$\frac{F(x)}{F_0} = (c1 + p1 \cdot x) \cdot \sin\left(\frac{2 \cdot \pi}{11}(x - 1985 - \pi)\right) + (c2 + p2 \cdot x), \quad (5)$$

where x is the date of interest in years, $F(x)$ the desired solar flux for that date, and F_0 is the solar flux at that wavelength

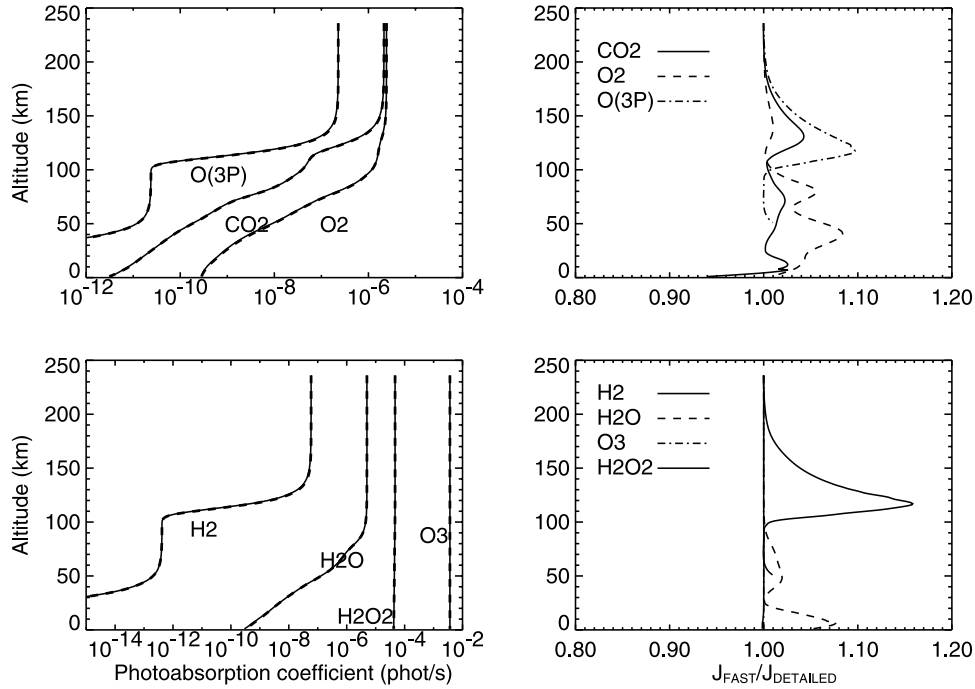

Figure 3. (left) Comparison between detailed model (solid lines) and fast scheme (dashed lines) for photoabsorption rates of (top) CO_2, O_2, and $O(^3P)$ and (bottom) H_2, H_2O, H_2O_2, and O_3. (right) Ratio fast to detailed results. See text for more details.

that was used in the computation of the tabulated photoabsorption rates. The parameters $c1$, $c2$, $p1$, and $p2$ are adjusted for each spectral interval and supplied to the program in tabulated form. They are included in Table 1. Future solar cycle data can be accommodated by changes in these four parameters only.

[27] Let us recall that this correction to the solar flux can be directly applied to the photoabsorption coefficients as they are directly proportional.

3.3. Comparison With Reference Model

[28] Results and CPU time consumption obtained using this UV tabulation have been compared with the detailed 1-D model described above. Figure 3 shows the photoabsorption coefficients for the seven absorbers mentioned above. The values given by the detailed and by the fast calculations are very similar in the upper atmosphere, the differences being lower than 10% in all cases, except for H_2. The biggest differences occur at those altitudes where there is a strong vertical gradient of the photoabsorption coefficient, since a slight difference can then lead to big fractional discrepancies. This is the case for H_2 between 100 and 150 km and for $O(^3P)$ around 120 km. Anyway, the impact of these two species on the total heating is small (see Figure 2). Excluding those altitudes, the comparison shows differences generally lower than 5%.

[29] The total heating rate obtained by the detailed model with different spectral resolutions (0.1, 1.0, and 10.0 nm) and by the fast scheme are compared in Figure 4. It can be seen that the precision achieved with this fast scheme is similar to that of the detailed model with a spectral resolution of 1 nm and even better below about 100 km. The CPU time consumed, however, is about 20 times lower. This saving is basically given by the number of intervals summed to perform the spectral integration and therefore not dependent on atmospheric conditions.

[30] We have also compared the heating rates obtained by the detailed model and by the fast scheme at different solar conditions (Figure 5). The variation of the total heating rate obtained between solar minimum and solar maximum is about 500 K/day at the altitude where the maximum heating occurs, and the fast scheme reproduces this solar cycle variation with high precision, with differences with the detailed model smaller than about 5%.

4. Photochemical Model

[31] Different models of the photochemistry of the Martian atmosphere have been developed in the last decades (see, for example, *Rodrigo et al.* [1990], *Moureau et al.* [1991], *Nair et al.* [1994], *Atreya and Gu* [1994], *Lefevre et al.* [2004]). Most of these models used the chemistry needed to take into account a diversity of tropospheric processes like the water vapor cycle or the ozone variability. In the upper atmosphere, however, the neutral chemistry can be usually simpler, with a reduced number of chemical reactions. In order to simplify those lower atmosphere models, we followed two main criteria. The first one was to account properly for the stability of the bulk Martian atmosphere, and therefore, to incorporate the most important catalytic cycles of recovery of CO_2. The second one was to build a self-consistent scheme for all the species involved, so that a steady state between productions and losses may be achieved. Our final scheme is detailed in Table 2 and includes the 12 major constituents of the C, O, and H families in the upper atmosphere (CO_2, O_2, $O(^3P)$, CO, H,

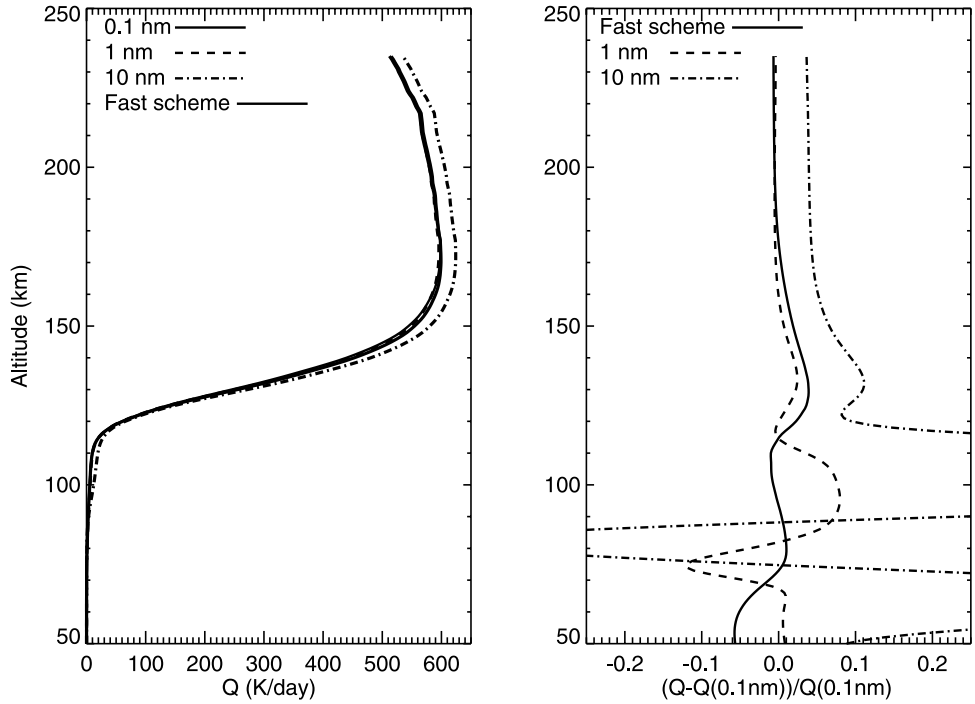

Figure 4. (left) Total heating rate, in K/day, obtained by the detailed model with three different spectral resolutions and by the fast scheme. (right) Differences with respect to the detailed model at the highest resolution (0.1 nm).

OH, HO_2, H_2, H_2O, H_2O_2, O_3, and $O(^1D)$), and 27 reactions between them, including photodissociations. No heterogeneous chemistry is considered.

[32] Although all the abundances needed are computed internally, any of them may be fixed externally or taken from other sources or models. This supplies flexibility and the possibility to couple it to more sophisticated chemical schemes at lower layers.

[33] Photodissociation rates needed for production and loss terms are computed and supplied by the UV solar

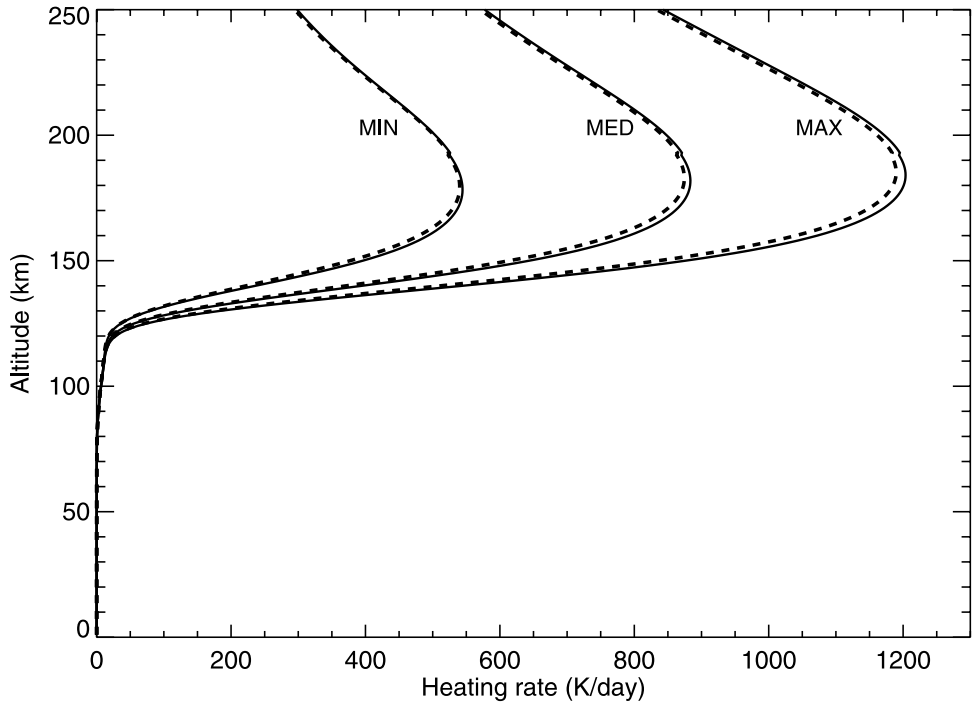

Figure 5. Total heating rate, in K/day, obtained by the detailed model (solid lines) and by the fast scheme (dashed lines) for minimum, medium, and maximum solar activity conditions, as indicated.

Table 2. Photochemical Reactions Included in the Model[a]

No.	Reaction	Rate	Reference
R1a	$CO_2 + h\nu \rightarrow CO + O$	computed	
R1b	$CO_2 + h\nu \rightarrow CO + O(^1D)$	computed	
R2	$H + O_2 + CO_2 \rightarrow HO_2 + CO_2$	$1.425 \cdot 10^{-31} \cdot \left(\frac{T}{300}\right)^{-1.6}$	1
R3	$O + HO_2 \rightarrow OH + O_2$	$3.0 \cdot 10^{-11} \cdot e^{200/T}$	1
R4	$CO + OH \rightarrow CO_2 + H$	$3.2 \cdot 10^{-13} \cdot e^{-300/T}$	2
R5	$2HO_2 \rightarrow H_2O_2 + O_2$	$2.3 \cdot 10^{-13} \cdot e^{600/T}$	1
R6	$H_2O_2 + h\nu \rightarrow 2OH$	computed	
R7	$OH + HO_2 \rightarrow H_2O + O_2$	$4.8 \cdot 10^{-11} \cdot e^{250/T}$	1
R8	$H_2O + h\nu \rightarrow H + OH$	computed	
R9	$O(^1D) + H_2O \rightarrow 2OH$	$2.2 \cdot 10^{-10}$	1
R10	$O + O + CO_2 \rightarrow O_2 + CO_2$	$1.1 \cdot 10^{-27} \cdot T^{-2.0}$	2
R11	$O + OH \rightarrow O_2 + H$	$2.2 \cdot 10^{-11} \cdot e^{120/T}$	1
R12a	$O_2 + h\nu \rightarrow 2O$	computed	
R12b	$O_2 + h\nu \rightarrow O + O(^1D)$	computed	
R13	$H + HO_2 \rightarrow H_2 + O_2$	$6.5 \cdot 10^{-12}$	2
R14	$O(^1D) + H_2 \rightarrow H + OH$	$1.1 \cdot 10^{-10}$	1
R15	$OH + H_2 \rightarrow H + H_2O$	$5.5 \cdot 10^{-1.2} e^{-2000/T}$	1
R18	$OH + H_2O_2 \rightarrow HO_2 + H_2O$	$2.9 \cdot 10^{-12} e^{-160/T}$	1
R19	$O(^1D) + CO_2 \rightarrow O + CO_2$	$7.4 \cdot 10^{-11} e^{120/T}$	1
R20	$O(^1D) + O_2 \rightarrow O + O_2$	$3.2 \cdot 10^{-11} e^{70/T}$	1
R21	$O + O_2 + CO_2 \rightarrow O_3 + CO_2$	$1.5 \cdot 10^{-33} T/300^{-2.4}$	1
R22	$O_3 + H \rightarrow OH + O_2$	$1.4 \cdot 10^{-10} e^{-470/T}$	1
R23	$O_3 + OH \rightarrow HO_2 + O_2$	$1.7 \cdot 10^{-12} e^{-940/T}$	1
R24	$O_3 + HO_2 \rightarrow OH + 2O_2$	$1.0 \cdot 10^{-14} e^{-490/T}$	1
R25a	$O_3 + h\nu \rightarrow O_2 + O$	computed	
R25b	$O_3 + h\nu \rightarrow O_2 + O(^1D)$	computed	
R27	$H_2 + h\nu \rightarrow 2H$	computed	

[a]References: 1, *Sander et al.* [2003]; 2, *Nair et al.* [1994].

absorption model described in previous sections. The absorption of solar radiation at the wavelengths considered can lead to two different effects: dissociation or ionization. While both channels contribute to the heating rate, only the dissociation is considered for the photochemistry. The dissociation-to-ionization branching ratios from *Torr et al.* [1979] were used for CO_2 and O_2. For the other constituents the absorption cross sections used here are always well above (H_2O, H_2O_2, and O_3) or well below ($O(^3P)$ and H_2) the ionization threshold.

[34] For the simulations presented here, the initial abundances are taken from *Nair et al.* [1994], although any arbitrary initial conditions can be used by the model. The reaction rates were taken from previous 1-D composition models [*Rodrigo et al.*, 1990; *Nair et al.*, 1994], with an update to the latest values available in the Jet Propulsion Laboratory (JPL) database [*Sander et al.*, 2003]. We maintained some modifications to these values within their error range, as proposed by *Nair et al.* [1994] in order to get a better agreement with observational results.

[35] Figure 6 shows the lifetime, i.e., the inverse of their specific losses, computed for all the constituents in the present photochemical model, for zenith conditions of solar illumination. As expected, most lifetimes increase with altitude as the pressure decreases. For those species whose dominant chemical loss is photolysis (like H_2O_2 and O_3), their lifetimes follow their photoabsorption profile, which may be constant in an ample range of altitudes.

[36] A common problem in photochemistry is that some of the compounds present very short lifetimes. It would be necessary to use very small time steps to solve their continuity equations, making the resolution very CPU time consuming. To avoid this problem, most of the photochemical models developed previously used the approximation of photochemical equilibrium (see, for example, *Rodrigo et al.* [1990]) for the time evolution of the shortest lived compounds. We also adopted this strategy in our model. For this purpose, and observing a clear gap (of almost 2 orders of magnitude) from the lifetimes of $O(^1D)$, OH, and HO_2 to those of the rest of species at most altitudes, we decided to

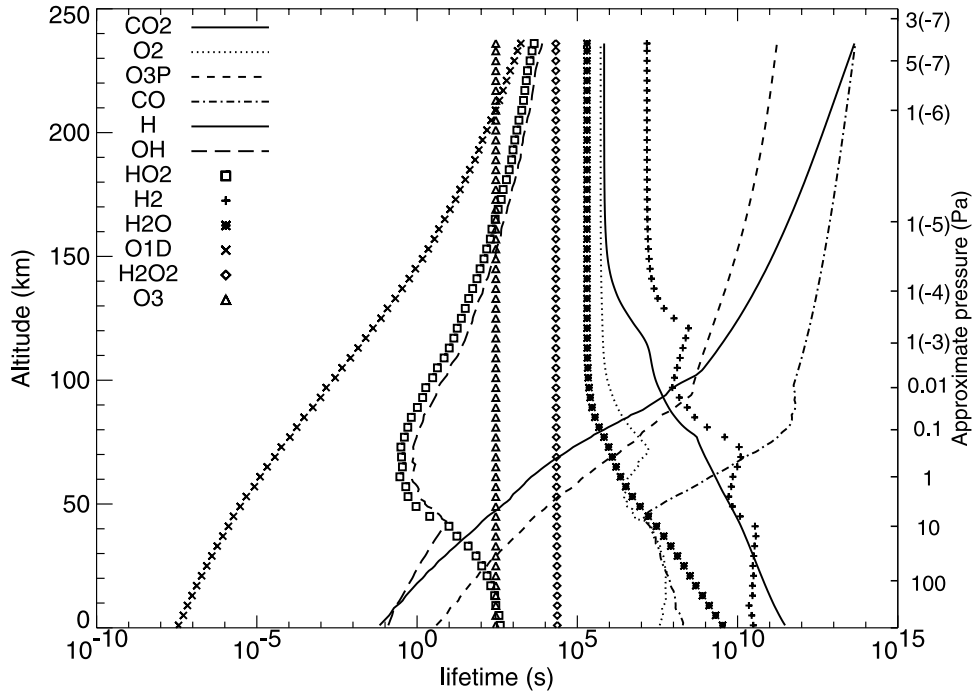

Figure 6. Photochemical lifetimes of several constituents in the upper Martian atmosphere. Zenith conditions. Solar medium activity.

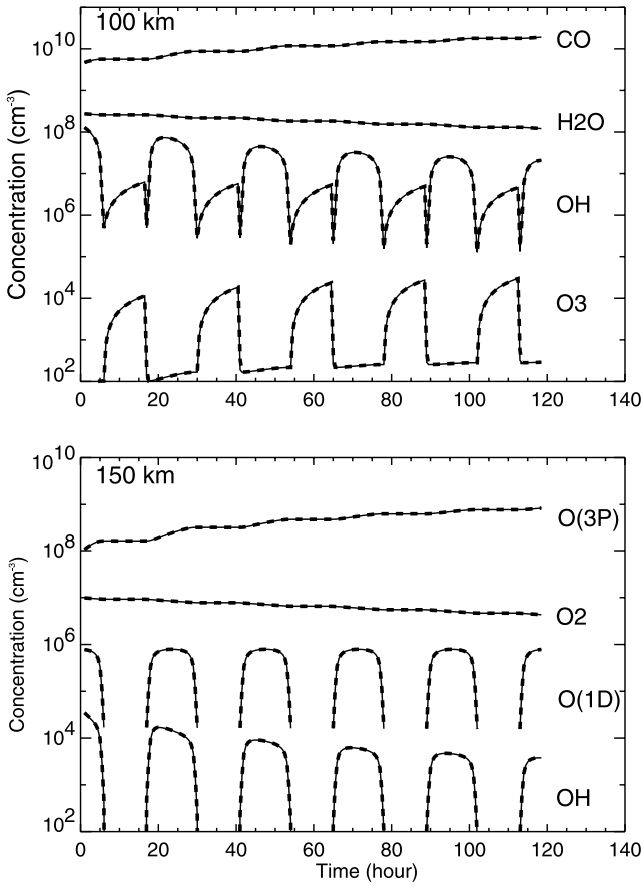

Figure 7. Evolution of diverse compounds at (top) 100 km and (bottom) 150 km given by the photochemical detailed model (solid lines) and the photochemical fast model (dashed lines).

assume photochemical equilibrium for these three species. The model's internal time step is chosen as a fraction of the shortest lifetime of the remaining species at each altitude, and a time-marching routine is followed to solve their continuity equations. The model's time step is much longer than the lifetimes of the three constituents in photochemical equilibrium, hence the condition for such an approximation is fulfilled.

[37] The internal time step is about 10^7 times larger than a calculation without this photochemical approximation at tropospheric and mesospheric altitudes, as it is essentially limited by ozone (see Figure 6). As a consequence, a similar reduction in the CPU time consumption is achieved. In the thermosphere the acceleration varies from 10^3 around 110 km to none around 200 km. These precise values will obviously vary for different background atmospheres. As it is given by the O_3 lifetime, that follows its photoabsorption coefficient profile, it can also be different for different solar conditions. However, the order of magnitude of the CPU time saving will be similar in all cases.

[38] The impact of this approximation on the model's results is shown in Figure 7, which compares the evolution of the concentrations of various species, at 100 and 150 km, with and without the assumption of photochemical equilibrium in the three fastest species mentioned above. It can be seen that this photochemical equilibrium assumption is a good approximation for the upper atmosphere of Mars, reproducing the nominal behavior very well with an important reduction in computation time, and not only for the compounds that present daily cycles, including those in photochemical equilibrium, but also for those with longer lifetimes.

5. Summary of the Fast Scheme and Implementation Guidelines

[39] The fast scheme proposed, consisting of two related modules, one for UV absorption and another for photochemistry, can be straightforwardly implemented in any GCM. All of the input variables needed by the subroutines are standard geophysical parameters in GCMs and are computed and available internally: concentration profiles of all the constituents, the temperature/pressure profile and the solar zenith angle or local time, in addition to the solar longitude, geographical latitude, etc. This information is passed to the fast scheme's subroutines at each point of the 3-D grid of the GCM. Then the scheme will perform the following steps. First, the column amounts in equation (2) are computed at the specified grid point and are used to interpolate in the look-up tables in order to obtain the partial photoabsorption coefficient of each compound for each of the 36 spectral subintervals. Second, the corrections in equations (3) and (4) for the temperature dependence of the CO_2 cross section and for the variation of the solar flux with the solar cycle (equation (5)) are applied in each subinterval to obtain the corrected partial photoabsorption coefficients, which are then summed to obtain the integrated photoabsorption coefficient for each constituent. Third, these coefficients are used for calculating the UV heating rate at the given grid point following equation (1) and sent back to the GCM. Now a second call at each grid point to the photochemical module follows. This procedure calculates all the chemical reaction rates in Table 2 using the actual temperature profile and uses the previous photoabsorption coefficients to compute also the photolysis rates. Then, it computes the changes in concentration of each constituent at the given point following a time marching method, except for $O(^1D)$, OH, and HO_2 which are solved with the approximation of photochemical equilibrium. Finally, these changes in concentration are passed back to the GCM. This approach allows for flexibility in calling the UV heating module and the photochemical module at different and variable time steps, depending on geophysical conditions and precision requirements. Notice that this scheme is local in nature, i.e., it operates at each altitude regardless of what the GCM does in the rest of the atmosphere. Therefore it can be used in conjunction with other chemical or transport schemes.

6. Application to the LMD-GCM

[40] The fast scheme described above for UV heating and for the photochemistry is already implemented and operative in the GCM developed at LMD and recently extended to the thermosphere [*Angelats i Coll et al.*, 2005]. Its implementation followed the guidelines given in the previous section, and it is used for the Martian mesosphere and thermosphere while another chemical scheme, extended to

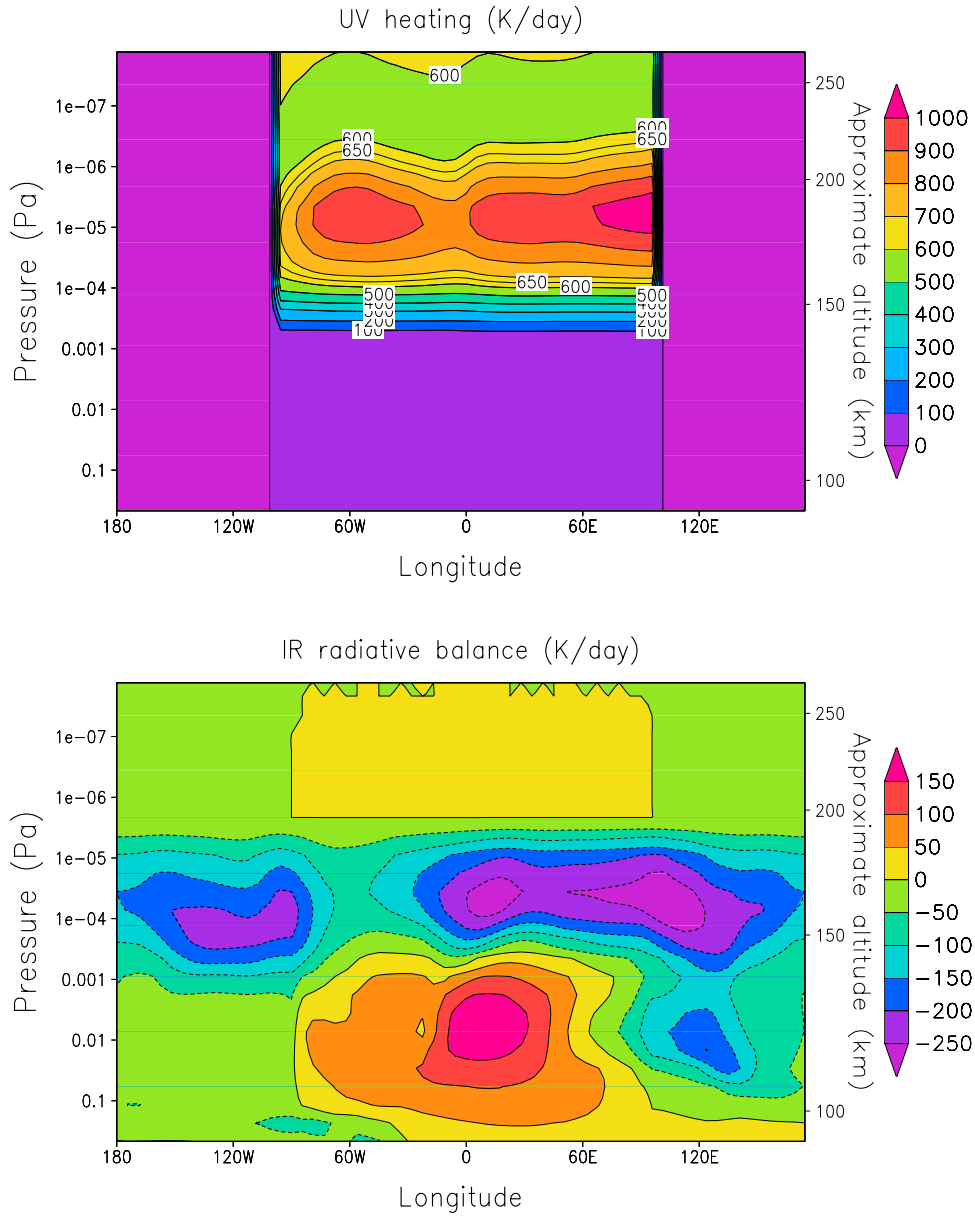

Figure 8. (top) UV heating and (bottom) IR balance in the equator; Ls = 0–30; solar medium conditions; UT = 1200; the two vertical lines are the morning and evening terminators.

more species and including some more reactions, can also be employed at lower layers [*Lefevre et al.*, 2004].

[41] In order to study the impact and behavior of the fast scheme within the LMD-GCM, a large number of simulations were performed. They belong to an extensive validation effort which is still ongoing, and only a selection of results are shown here. Although these selected results can be considered as preliminary at its smallest scales and features, in our opinion the overall behavior is consolidated, based on the reproduction of expected trends and in view of the similarity with previous models, as we will mention below. They also illustrate the potential of an upward extension of a Martian GCM like this. The GCM was run for 18 "Martian months", starting from $L_s = 0$. We analyze here results after one Martian year of simulation time, that is, for the 13th Martian month, for which L_s varies between 0 and 30, the results corresponding to averages during that period.

[42] Figures 8 and 9 show the relative importance of the diverse radiative heating terms obtained in the upper atmosphere with this LMD-GCM. Figure 8 shows that, below 0.001 Pa, the UV heating is negligible and the IR radiative balance (including near-IR solar heating and CO_2 15-μm cooling, using a rate coefficient for thermal collisions between CO_2 and O of 3^{-12} cm^3s^{-1} following [*López-Puertas et al.*, 1992] and in line with the values used in the three terrestrial thermospheres [*Bougher and Roble*, 1991; *Fox*, 1988]) is the dominant radiative forcing. At higher layers the IR balance is controlled by the 15-μm cooling and the UV heating begins to be dominant. The energy balance at noon can be better appreciated in Figure 9, which shows how the UV heating is compensated below 10^{-4} Pa by both

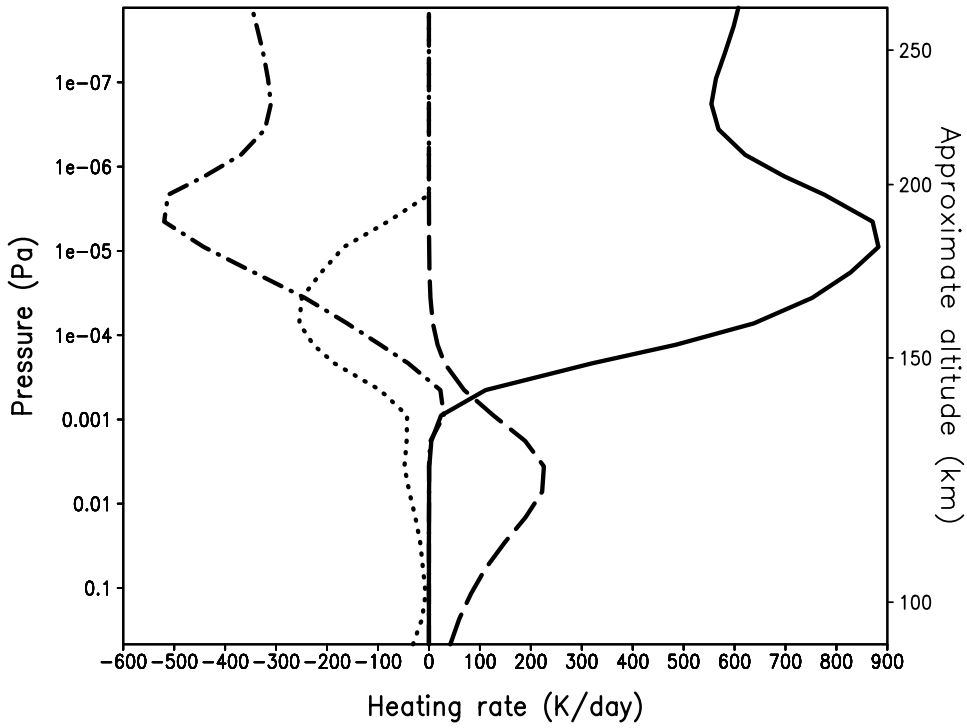

Figure 9. Equatorial profiles of heating and cooling terms at midday. Solid: UV heating; dashed: NIR radiative heating; dotted: 15 μm radiative cooling; dotted-dashed: thermal conduction; Ls = 0–30; solar medium conditions.

IR cooling and thermal conduction, and by mainly thermal conduction above. The longitudinal structure of the UV heating, which shows two areas of maximum heating, one focused at longitude 60W and the other one at the evening terminator, is related to the structure obtained in the O/CO_2 ratio, which is presented in Figure 10. This is due to the higher efficiency of CO_2 compared to atomic oxygen in absorbing UV radiation and thus in heating the atmosphere. This effect shows the importance of the photochemistry for the thermal structure of the upper atmosphere, as will be shown below.

[43] The thermal structure obtained is in qualitative agreement with that obtained by *Bougher et al.* [1999] with the MTGCM. However, our peak UV heating is lower than

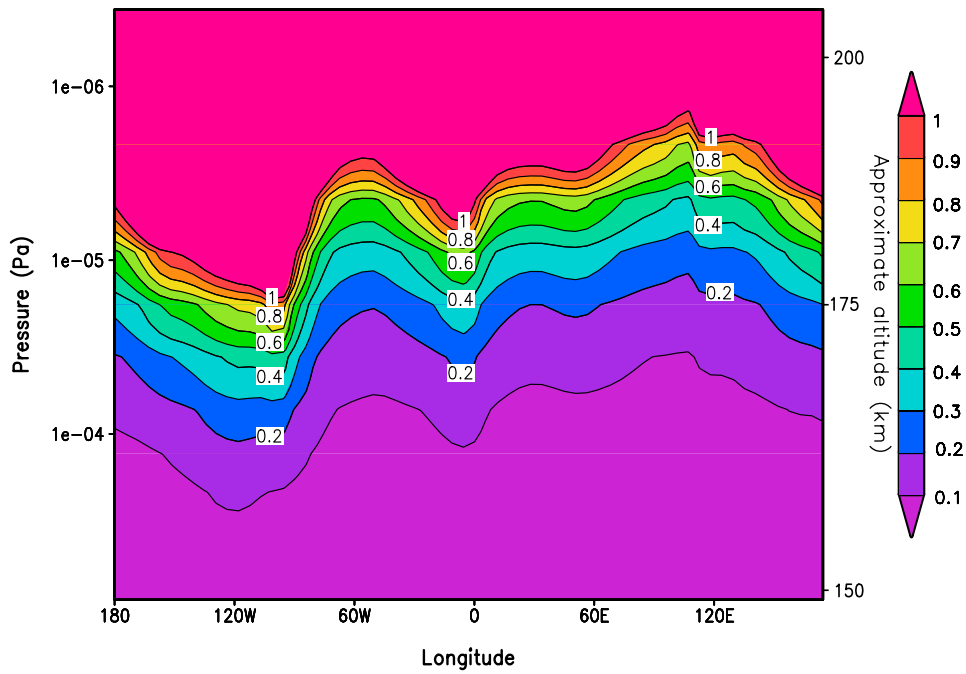

Figure 10. Equatorial profile of O/CO_2 ratio; Ls = 0–30; solar medium conditions; UT = 1200.

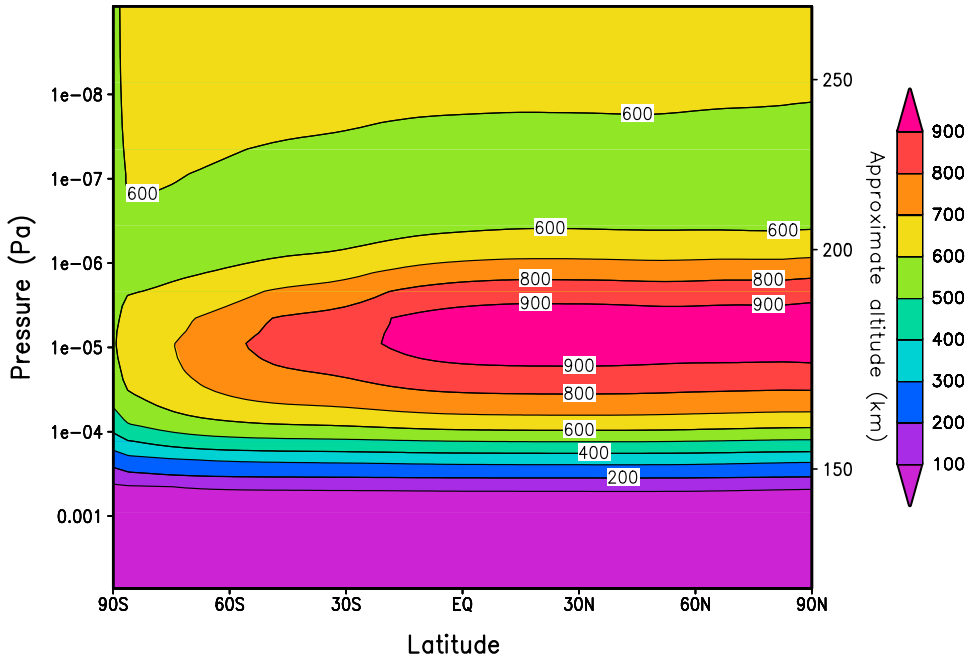

Figure 11. Zonal mean daytime UV heating at UT = 1200; Ls = 0–30; solar medium conditions.

the MTGCM (900 K versus 1300 K). This can be due to several factors: while our model is consistently coupled with the lower layers, Bougher and coworkers prescribed tidal parameters given by the NASA-Ames MGCM in the MTGCM lower boundary, probably affecting in different ways the thermospheric temperature. A new scheme for coupling of the MTGCM to lower altitudes has been used [*Bougher et al.*, 2004], but no useful data for this comparison is yet published. Additionally, our photochemical scheme is different to that used in the MTGCM. As will be shown below, this can have an important effect over the UV heating. However, a detailed comparison between both models would eventually be useful to understand better these differences.

[44] We can see in Figure 11 the latitude-pressure map of zonal mean daytime UV heating for UT = 1200. The maximum UV heating, in K/day, is produced in a narrow layer at a pressure level of about 10^{-5} Pa, as a consequence of the competition between the downward decreasing heating (in volumic units) and the upward decreasing density. This maximum value is of about 900 K. Simulations (not shown here) show that the altitude of the peak heating does not change significantly with solar cycle. Figure 12 shows the profile of zonal mean daytime temperature for the same conditions. As expected, the temperature is constant with altitude in the uppermost layers. The altitude at which UV heating begins to dominate the heating balance (about 10^{-3} Pa in Figures 8 and 9) can be identified in the temperature plot as the altitude at which a steep increase in temperature occurs. The zonal mean daytime temperature in the northern polar region is higher than in the southern polar region because the average used to plot the results, as indicated above, is displaced to the Northern summer (centered in Ls = 15).

[45] The seasonal standard deviation (SD) of the zonal mean daytime temperatures, shown in Figure 13, shows that the SD is small, usually below about 5% of the mean temperature, except at high latitudes. This is expected since at those latitudes illumination conditions change quickly for small changes in L_s. Except for this case, the day-to-day variation is small, not affecting in an important way the validity of the results shown here.

[46] As stated before, our photochemical model only considers neutral compounds so far, neglecting thus the effects of the ionosphere over the neutral atmosphere. The creation of atomic oxygen by dissociative recombination, $O_2^+ + e^- \rightarrow O + O$ is one of these effects [*Schunk and Nagy*, 2000]. So, our model can be underestimating the atomic oxygen concentration. In fact, comparisons of our results with the O mixing ratio deduced by [*Hanson et al.*, 1977] and [*Stewart et al.*, 1992] from measurements from Viking and Mariner 9, respectively, show that our O mixing ratio tends to be underestimated in about 50% at the dayside ionospheric peak. For the purpose of comparisons with previous results, we have approximately estimated this error in the following way. First, we have supposed that all the CO_2^+ produced in the photoionization of CO_2 is instantaneously converted to O_2^+ due to the reaction $CO_2^+ + O \rightarrow CO + O_2^+$ and that all this O_2^+ is rapidly converted to O by dissociative recombination. Following *Fox and Dalgarno* [1979] almost all this atomic oxygen will be formed in the state $O(^1D)$. Within these assumptions, the final result of a CO_2 ionization would be $CO_2 + h\nu \rightarrow CO + O(^1D)$, that is, similar to reaction 1b in Table 2. Calculations with our 1-D model show that the CO_2 photoionization rate is between 50% and 75% that of the reaction 1b, so to obtain an upper boundary estimation of the effect of the ionosphere over the atomic oxygen concentration we have simply duplicated the rate of reaction 1b and repeated the simulation for solar medium conditions. Results (not shown here) show that the effect of this modification over the O mixing ratio is small, increasing it by about 10%. This improves the comparison with the experimental results, but a good agreement is not yet achieved. In the future, after incorporating a more

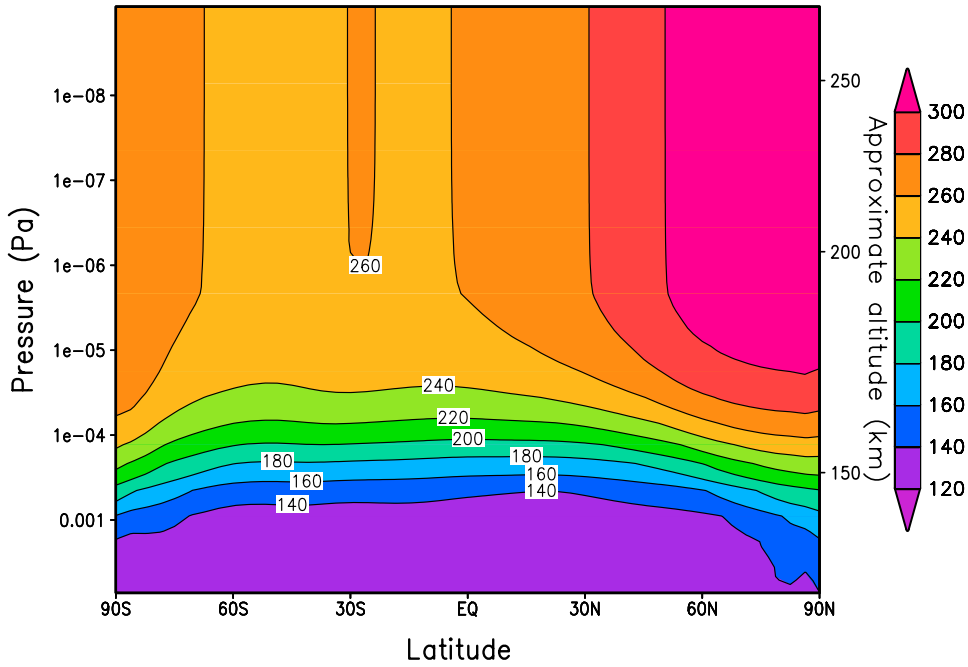

Figure 12. Zonal mean daytime temperature at UT = 1200; Ls = 0–30; solar medium conditions.

complete ionospheric module, a more detailed comparison, using conditions and dust loading appropriate for Mariner 9 and Viking, will be needed to clarify these differences.

[47] We have also studied the overall effect of the photochemistry on the thermal structure of the upper atmosphere. Such an effect is expected, as photochemistry is clearly linked to the UV heating of the atmosphere. In order to evaluate this interaction, we have run the GCM for the Martian month 13 without photochemistry, that is, starting with the final conditions of the month 12, and ignoring changes in composition from the photodissociations and chemical reactions listed in Table 2 from that moment onward. The difference in the zonal mean daytime temperatures obtained between both runs (temperature without photochemistry "NOPH" minus the nominal temperature including photochemistry "NOM") can be seen in Figure 14. This difference is very small below the mesopause, about 10^{-4} Pa or 110 km, and only begins to be important in the

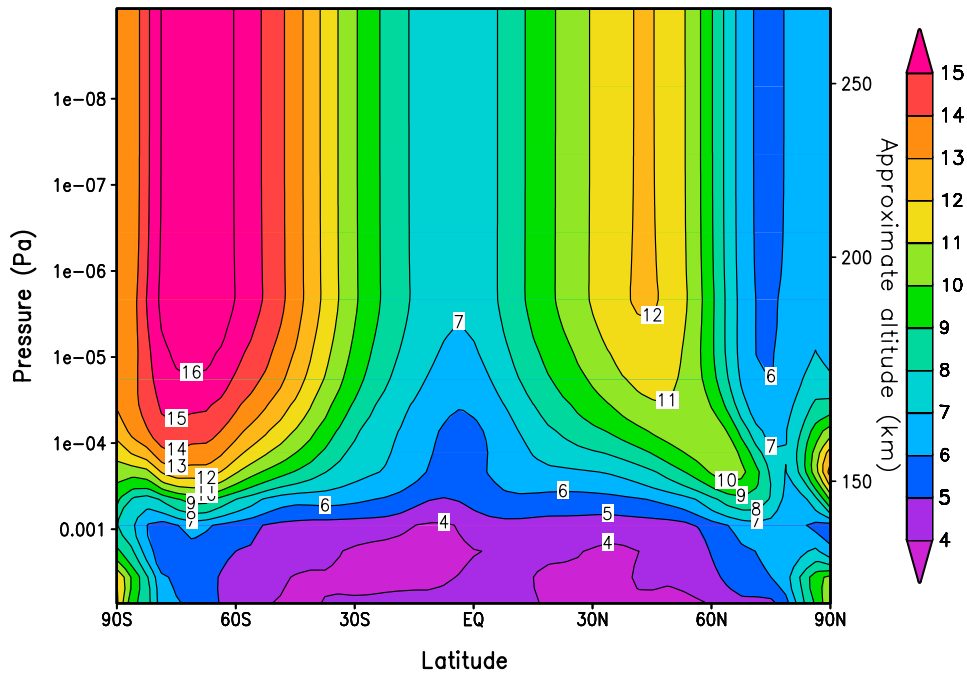

Figure 13. Zonal mean daytime standard deviation of the temperature at UT = 1200; Ls = 0–30; solar medium conditions.

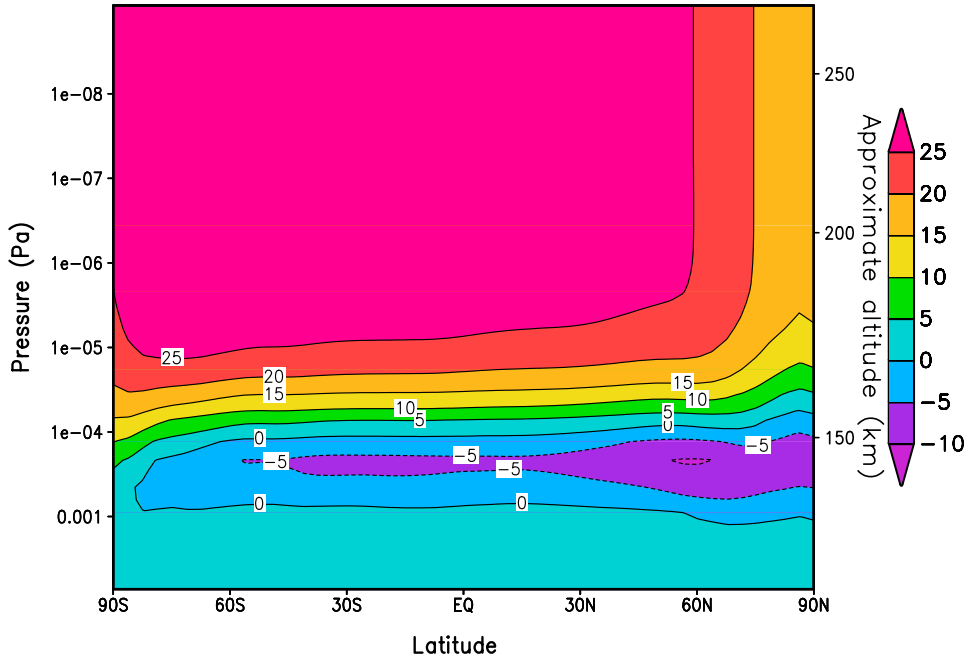

Figure 14. Difference in zonal mean daytime temperature between the run without photochemistry and the run with photochemistry, UT = 1200; Ls = 0–30; solar medium conditions.

region where the UV heating is the dominant heating source (see Figure 9). The case "NOPH" is warmer, with a maximum difference of about 25 K in the upper thermosphere. To study the origin of this difference in temperature, we have plotted, in Figure 15, the differences in the CO_2 mixing ratio obtained between both runs and in Figure 16 the impact on the UV heating. Since one of the most important effects of photochemistry in the upper atmosphere is the photolysis of CO_2, it is no surprise that this species is more abundant in the "NOPH" simulation, and since CO_2 is more efficient than atomic oxygen in absorbing UV radiation (over a wider wavelength range and with higher cross section), the results in Figures 15 and 16 agree with the expected trend.

[48] Another thermospheric result from this extended GCM is the sensitivity of the temperature at these altitudes to the solar cycle, as information from previous studies is available. Three simulations with solar fluxes appropriate

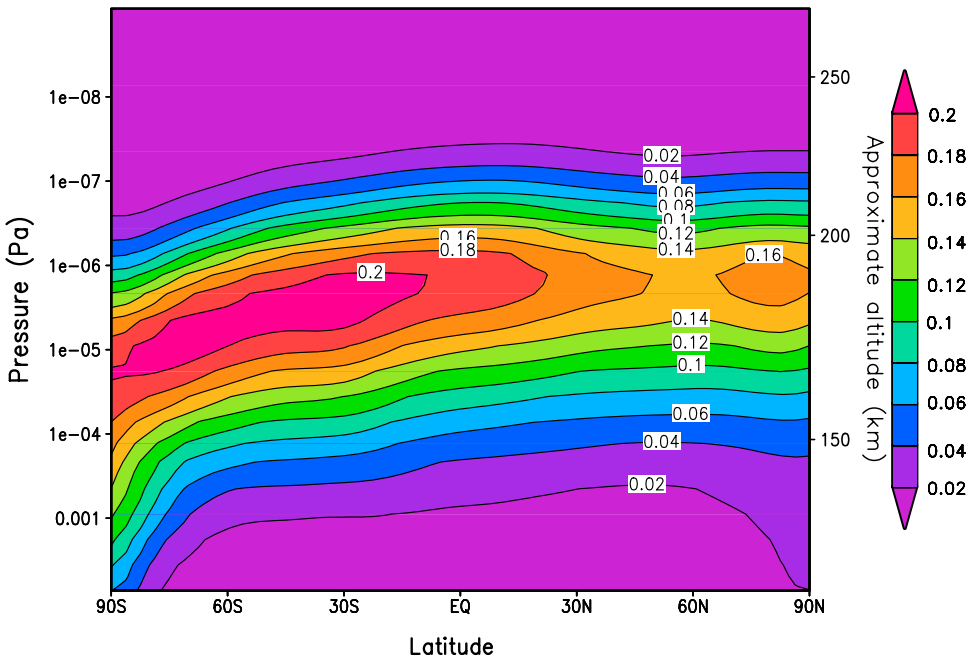

Figure 15. Difference in zonal mean daytime CO_2 mixing ratio between the run without photochemistry and the run with photochemistry, UT = 1200; Ls = 0–30; solar medium conditions.

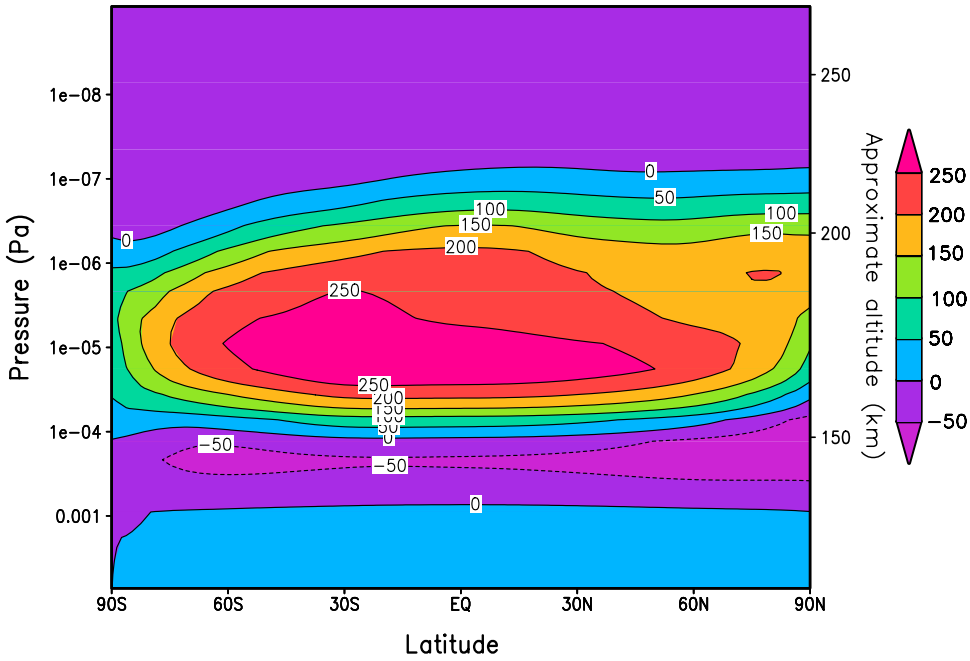

Figure 16. Difference in zonal mean daytime UV heating between the run without photochemistry and the run with photochemistry, UT = 1200; Ls = 0–30; solar medium conditions.

for solar minimum, medium and maximum conditions were performed. The maximum daytime and minimum nighttime temperatures obtained for the three conditions are shown in Figure 17. This figure is directly comparable to Figure 4a of *Bougher et al.* [1999], from where their global average temperatures can be estimated as ≈247 K for solar maximum, ≈217 K for solar average and ≈184 K for solar minimum. Estimating in the same way our global mean temperatures, the values obtained are about 279 K, 227 K, and 166 K, respectively, showing a larger variability. Maximum daytime temperatures agree quite well, although for solar maximum conditions our temperature is higher. Our minimum nighttime temperatures show a higher variability than those of *Bougher et al.* [1999], our temperatures being higher for solar maximum conditions and lower for solar minimum. As explained by *Bougher et al.* [2000] the scarcity of data from spacecrafts, specially for solar maximum conditions and for nighttime temperatures makes difficult to constrain this solar cycle evolution. A detailed intercomparison of GCMs at thermospheric altitudes would also be very useful.

7. Conclusions and Future Work

[49] Fast schemes for the calculation of UV heating and photochemistry suitable to be implemented in a generic GCM of the Martian atmosphere have been presented. They have been developed using as a reference more detailed routines included in a 1-D model of the Martian upper atmosphere, after introducing parameterizations and approximations to make them suitable to be included in a GCM without consuming much CPU time.

[50] The fast scheme for the UV heating proposed uses a tabulation of the photoabsorption coefficients obtained by the UV detailed model and is based on the small dependence of the cross sections with temperature and pressure in selected spectral subintervals. Corrections in order to include the variation of the solar flux during the 11-year solar cycle and the temperature dependence of the CO_2 cross section have also been included. The photoabsorption coefficients and the heating rates obtained are satisfactorily compared to those given by the detailed model, and the CPU consumption is around 200 times smaller than for the detailed model using 0.1 nm resolution.

[51] The photochemical model allows the study of the variations of the most important compounds of the C, O, and H families in the upper atmosphere, by using the 12

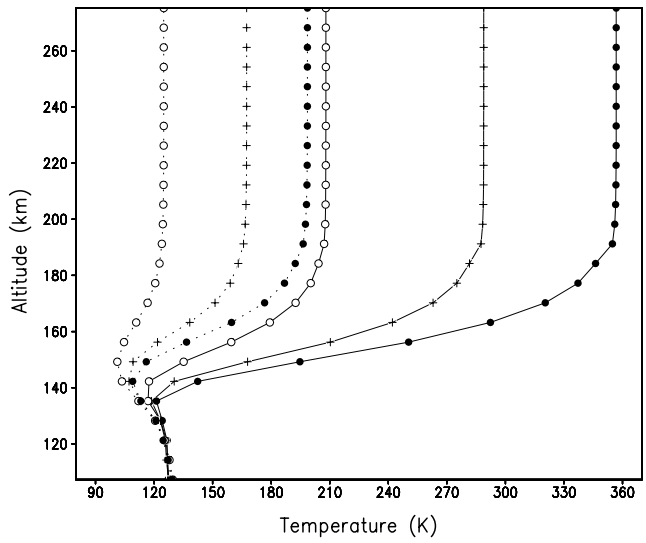

Figure 17. Maximum daytime (solid lines) and minimum nighttime (dotted lines) temperatures for solar maximum (solid circles), solar medium (crosses), and solar minimum (open circles) conditions; Ls = 0–30.

constituents (CO_2, O_2, $O(^3P)$, CO, H, OH, HO_2, H_2, H_2O, H_2O_2, O_3, and $O(^1D)$) and the 27 reactions between them listed in Table 2. We propose, as most previous models do, the use of the approximation of photochemical equilibrium in three species: $O(^1D)$, OH, and HO_2, and it is shown that this leads to accurate results and at the same time to important CPU time savings. This CPU acceleration is higher in the lower and middle atmosphere, where the lifetimes of the three fastest species are smallest.

[52] Future improvements are foreseen for both the 1-D detailed models used as a reference and in the fast schemes, as for example in the extension to new UV absorbers, the update of cross sections or the addition of chemical reaction rates of secondary importance. In principle, any improvement introduced into the detailed model is susceptible to be included in the fast methods following the strategies explained in section 5.

[53] These fast schemes have been already implemented in the GCM developed at the LMD, which has become the first single GCM to cover the Martian atmosphere from the ground to the exosphere. This opens perspectives to study new aspects of the atmosphere, like the coupling between different processes that act at different altitudes. Moreover, this extension will allow to create a new version of the European Mars Climate Database, including the thermosphere, that will be useful for the design of future aerobraking maneuvers.

[54] In this work we have used this extended LMD-GCM to illustrate some problems of the Martian upper atmosphere. We have studied the thermal balance of the upper atmosphere, obtaining a qualitative agreement with results of *Bougher et al.* [1999]. Explanations for the quantitative differences have been proposed, although a detailed comparison between both models would be needed to fully understand them. The effect of the photochemistry on the thermospheric temperatures has also been considered, and we have shown that its inclusion affects them due to changes (increases) in the O/CO_2 ratio; as CO_2 heats the atmosphere more effectively than atomic oxygen, higher O/CO_2 ratios mean lower temperatures in the thermosphere. This result quantifies the sensitivity of the upper atmosphere to composition changes at those altitudes and indicates the need of appropriate photochemical schemes. The variation of thermospheric temperatures during the solar cycle has also been studied. The agreement is good, but our model shows a higher variability. Future detailed intercomparisons between thermospheric GCMs will be very useful to clarify this effect.

[55] Once more we recall that more validation work of the present GCM is ongoing, including further comparisons with other models and with results from different missions, as well as sensitivity tests that will hopefully reveal and quantify the further interactions between different processes over the thermosphere.

[56] **Acknowledgments.** This research was funded under CNES Mars Premier Program and ESTEC contract 11369/95/NL/J. Francisco González-Galindo is supported by an I3P Individual Fellowship from the "Consejo Superior de Investigaciones Cientificas" (CSIC) at the IAA.

References

Anbar, A. D., M. Allen, and H. A. Nair (1993), Photodissociation in the atmosphere of Mars: Impact of high resolution, temperature-dependent CO_2 cross-section measurements, *J. Geophys. Res.*, *98*, 10,925–10,931.

Angelats i Coll, M., F. Forget, F. Hourdin, Y. Wanherdrick, M. A. López-Valverde, F. González-Galindo, P. L. Read, and S. R. Lewis (2003a), Towards a global model of the Martian atmosphere, paper presented at International Workshop: Mars Atmosphere Modelling and Observations, Eur. Space Agency, Granada, Spain, 13–15 Jan.

Angelats i Coll, M., F. Forget, F. Hourdin, Y. Wanherdrick, M. A. López-Valverde, F. González-Galindo, S. R. Lewis, and P. L. Read (2003b), The Mars Thermospheric LMD General Circulation Model: First comparisons with MGS aerobraking data, paper presented at DPS Meeting 35, Am. Astron. Soc., Monterey, Calif.

Angelats i Coll, M., F. Forget, M. A. López-Valverde, P. L. Read, and S. Lewis (2004), Upper atmosphere of Mars up to 120 km: Mars Global Surveyor accelerometer data analysis with the LMD general circulation model, *J. Geophys. Res.*, *109*, E01011, doi:10.1029/2003JE002163.

Angelats i Coll, M., F. Forget, M. A. López-Valverde, and F. González-Galindo (2005), The first Mars thermospheric general circulation model: The Martian atmosphere from the ground to 240 km, *Geophys. Res. Lett.*, *32*, L04201, doi:10.1029/2004GL021368.

Atreya, S. K., and Z. G. Gu (1994), Stability of the Martian atmosphere: Is heterogeneous catalysis essential?, *J. Geophys. Res.*, *99*, 13,133–13,145.

Banks, P. M., and G. Kockarts (1973), *Aeronomy, Part A*, Elsevier, New York.

Basu, S., M. I. Richardson, and R. J. Wilson (2004), Simulation of the Martian dust cycle with the GFDL Mars GCM, *J. Geophys. Res.*, *109*, E11006, doi:10.1029/2004JE002243.

Bougher, S. W., and R. E. Dickinson (1988), Mars mesosphere and thermosphere: 1. Global mean heat budget and thermal structure, *J. Geophys. Res.*, *93*, 7325–7337.

Bougher, S. W., and R. G. Roble (1991), Comparative terrestrial planet thermospheres, 1, Solar cycle variation of global mean temperatures, *J. Geophys. Res.*, *96*, 11,045–11,055.

Bougher, S. W., R. G. Roble, E. C. Ridley, and R. E. Dickinson (1990), The Mars thermosphere: 2. General circulation with coupled dynamics and composition, *J. Geophys. Res.*, *95*, 14,811–14,827.

Bougher, S. W., S. Engel, R. G. Roble, and B. Foster (1999), Comparative terrestrial planet thermospheres 2. Solar cycle variation of global structure and winds at equinox, *J. Geophys. Res.*, *104*, 16,591–16,611.

Bougher, S. W., S. Engel, R. G. Roble, and B. Foster (2000), Comparative terrestrial planet thermospheres 3. Solar cycle variation of global structure and winds at solstices, *J. Geophys. Res.*, *105*, 17,669–17,692.

Bougher, S. W., S. Engel, D. P. Hinson, and J. M. Forbes (2001), Mars Global Surveyor Radio Science electron density profiles: Neutral atmosphere implications, *Geophys. Res. Lett.*, *28*, 3091–3094.

Bougher, S. W., S. Engel, D. P. Hinson, and J. R. Murphy (2004), MGS Radio Science electron density profiles: Interannual variability and implications for the Martian neutral atmosphere, *J. Geophys. Res.*, *109*, E03010, doi:10.1029/2003JE002154.

Brasseur, G., and S. Solomon (1986), *Aeronomy of the Middle Atmosphere*, 2nd ed., D. Reidel, Norwell, Mass.

Chipperfield, M. P. (1999), Multiannual simulations with a three-dimensional chemical transport model, *J. Geophys. Res.*, *104*, 1781–1805.

Crowley, G., M. A. Bullock, C. Freitas, D. Boice, L. Young, D. H. Grinspon, R. Gladstone, R. Link, and W. Huebner (2003), Development of a surface-to-exosphere Mars atmosphere model, paper presented at International Workshop: Mars Atmosphere Modelling and Observations, Eur. Space Agency, Granada, Spain, 13–15 Jan.

Donnelly, R. F., H. E. Hinteregger, and D. F. Heath (1986), Temporal variation of solar EUV, UV, and 10830-A radiation, *J. Geophys. Res.*, *91*, 5567–5578.

Dyominov, I. G., and A. M. Zadorozhny (2001), Contribution of solar UV radiation to the observed ozone variations during the 21st and 22nd solar cycles, *Adv. Space Res.*, *27*(12), 1949–1954.

Forget, F., F. Hourdin, and O. Talagrand (1998), CO_2 snowfall on Mars: Simulation with a General Circulation Model, *Icarus*, *131*, 302–316.

Forget, F., F. Hourdin, R. Fournier, C. Hourdin, and O. Talagrand (1999), Improved general circulation models of the Martian atmosphere from the surface to above 80 km, *J. Geophys. Res.*, *104*, 24,155–24,175.

Fox, J. L. (1988), Heating efficiencies in the thermosphere of Venus reconsidered, *Planet. Space Sci.*, *36*, 37–46.

Fox, J. L., and S. W. Bougher (1991), Structure, luminosity and dynamics of the Venus thermosphere, *Space Sci. Rev.*, *55*, 357–489.

Fox, J. L., and A. Dalgarno (1979), Ionization, luminosity and heating of the upper atmosphere of Mars, *J. Geophys. Res.*, *84*, 7315–7330.

Fox, J. L., and A. Dalgarno (1981), Ionization, luminosity and heating of the upper atmosphere of Venus, *J. Geophys. Res.*, *86*, 629–639.

Haberle, R. M., J. B. Pollack, J. R. Barnes, R. W. Zurek, C. B. Leovy, J. R. Murphy, H. Lee, and J. Schaeffer (1993), Mars atmospheric dynamics as

simulated by the NASA Ames General Circulation Model: 1. The zonal-mean circulation, *J. Geophys. Res.*, *98*, 3093–3123.

Haberle, R. M., J. R. Barnes, J. R. Murphy, M. M. Joshi, and J. Schaeffer (1997), Meteorological predictions for the Mars Pathfinder lander, *J. Geophys. Res.*, *102*, 13,301–13,311.

Haberle, R. M., M. M. Joshi, J. R. Murphy, J. R. Barnes, J. T. Schofield, G. Wilson, M. A. Lpez-Valverde, J. L. Hollinngsworth, A. F. C. Bridger, and J. Schaeffer (1999), General circulation model simulations of the Mars Pathfinder atmospheric structure investigation/meteorology data, *J. Geophys. Res.*, *104*, 8957–8974.

Hanson, W. B., S. Sanatani, and D. R. Zuccaro (1977), The Martian ionosphere as observed by the Viking Retarding Potential Analyzers, *J. Geophys. Res.*, *82*, 4351–4363.

Heroux, L. J., and H. E. Hinteregger (1985), Solar ultraviolet irradiance, in *Handbook of Geophysics and the Space Environment*, edited by A. S. Jurna, pp. 2-1 to 2-21, Air Force Geophys. Lab., Hancom Air Force Base, Mass.

Hinson, D. P., and R. J. Wilson (2004), Temperature inversions, thermal tides, and water ice clouds in the Martian tropics, *J. Geophys. Res.*, *109*, E01002, doi:10.1029/2003JE002129.

Holton, J. R. (1992), *An Introduction to Dynamic Meteorology*, Elsevier, New York.

Houghton, J. T. (1977), *The Physics of Atmospheres*, Cambridge Univ. Press, New York.

Hourdin, F., P. Le Van, F. Forget, and O. Talagrand (1993), Meteorological variability and the annual surface pressure cycle on Mars, *J. Atmos. Sci.*, *50*, 3625–3640.

Hourdin, F., F. Forget, R. Fournier, O. Talagrand, P. L. Read, M. Collins, S. R. Lewis, N. P. J. Thomas, and J.-P. Huot (1996), Numerical modelling of the general circulation of the Martian atmosphere, paper presented at Proceedings on Environment Modelling for Space-Based Application, Eur. Space Res. and Technol. Cent., Noordwijk, Netherlands.

Joshi, M., R. Haberle, J. Hollingsworth, and D. Hinson (2000), A comparison of MGS Phase 1 aerobraking radio occultation data and the NASA Ames Mars GCM, *J. Geophys. Res.*, *105*, 17,601–17,615.

Lean, J. (1987), Solar ultraviolet irradiance: A review, *J. Geophys. Res.*, *92*, 839–868.

Lefevre, F., S. Lebonnois, F. Montmessin, and F. Forget (2004), Three-dimensional modeling of ozone on Mars, *J. Geophys. Res.*, *109*, E07004, doi:10.1029/2004JE002268.

Lewis, S. R., M. Collins, P. L. Read, F. Forget, F. Hourdin, R. Fournier, C. Hourdin, O. Talagrand, and J. P. Huot (1999), A climate database for Mars, *J. Geophys. Res.*, *104*, 24,177–24,194.

López-Puertas, M., M. A. López-Valverde, C. P. Rinsland, and M. R. Gunson (1992), Analysis of the upper atmosphere $CO_2(\nu_2)$ vibration temperatures retrieved from ATMOS-Spacelab 3 observations, *J. Geophys. Res.*, *97*, 20,469–20,478.

López-Valverde, M. A., D. P. Edwards, M. López-Puertas, and C. Roldán (1998), Non-local thermodynamic equilibrium in general circulation models of the Martian atmosphere: 1. Effects of the local thermal equilibrium approximation on thermal cooling and solar heating, *J. Geophys. Res.*, *103*, 16,759–16,870.

López-Valverde, M. A., R. M. Haberle, and M. López-Puertas (2000), Non-LTE radiative mesospheric study for Mars Pathfinder entry, *Icarus*, *146*, 360–365.

López-Valverde, M. A., F. González-Galindo, F. Lefevre, S. Lebonnois, T. Moffat, A. D. Aylward, and S. W. Bougher (2003), Inter-comparison of UV radiation models in the upper atmosphere of Mars, paper presented at International Workshop: Mars Atmosphere Modelling and Observations, Eur. Space Agency, Granada, Spain, 13–15 Jan.

Mouden, Y., and J. C. McConnell (2005), A new model for multiscale modeling of the Martian atmosphere, GM3, *J. Geophys. Res.*, *110*, E04001, doi:10.1029/2004JE002354.

Moureau, D., L. W. Esposito, and G. Brasseur (1991), The chemical composition of the dust-free Martian atmosphere: Preliminary results of a two-dimensional model, *J. Geophys. Res.*, *96*, 7933–7945.

Nair, H., M. Allen, A. D. Anbar, and Y. L. Yung (1994), A photochemical model of the Martian atmosphere, *Icarus*, *111*, 124–150.

Parkinson, W. H., and K. Yoshino (2003), Absorption cross-section measurements of water vapor in the wavelength region 181–199 nm, *Chem. Phys.*, *294*, doi:10.1016/S0301-0104(03)00361-6.

Parkinson, W. H., J. Rufus, and K. Yoshino (2003), Absolute absorption cross section measurements of CO_2 in the wavelength region 163–200 nm and the temperature dependence, *Chem. Phys.*, *290*, doi:10.1016/S0301-0104(03)00146-0.

Pollack, J. B., R. M. Haberle, J. Schaeffer, and H. Lee (1990), Simulations of the general circulation of the Martian atmosphere: 1. Polar processes, *J. Geophys. Res.*, *95*, 1447–1474.

Richardson, M. I., and R. J. Wilson (2002), Investigation of the nature and stability of the Martian seasonal water cycle with a general circulation model, *J. Geophys. Res.*, *107*(E5), 5031, doi:10.1029/2001JE001536.

Ridley, A. J., G. Toth, and S. Bougher (2004), The Global Ionosphere Thermosphere Model and its applications to planetary atmospheres, *Eos Trans. AGU*, *85*(17), Abstract SA41A-06.

Roble, R. G., and B. A. Emery (1983), On the global mean temperature of the thermosphere, *Planet. Space Sci.*, *31*, 597–614.

Rodrigo, R., E. García-Álvarez, M. J. López-González, and J. J. López-Moreno (1990), A nonsteady one-dimensional theoretical model of Mars' neutral atmospheric composition between 30 and 200 km, *J. Geophys. Res.*, *95*, 14,795–14,810.

Sander, S. P., R. R. Friedl, D. M. Golden, M. J. Kurylo, R. E. Huie, V. L. Orkin, A. R. Ravishankara, C. E. Kolb, and M. J. Molina (2003), Chemical kinetics and photochemical data for use in atmospheric studies, eval. 14, *JPL Publ., 02-25*.

Schunk, R. W., and A. F. Nagy (2000), *Ionospheres: Physics, Plasma Physics and Chemistry*, Cambridge Univ. Press, New York.

Smith, D. E., M. T. Zuber, R. M. Haberle, D. D. Rowlands, and J. R. Murphy (1999), The Mars seasonal CO_2 cycle and the time variation of the gravity field: A general circulation model simulation, *J. Geophys. Res.*, *104*, 1885–1896.

Stewart, A. I. F., M. J. Alexander, R. R. Meier, L. J. Paxton, S. W. Bougher, and C. G. Fesen (1992), Atomic oxygen in the Martian thermosphere, *J. Geophys. Res.*, *97*, 91–102.

Tobiska, W. K., T. Woods, F. Eparvier, R. Viereck, L. Floyd, D. Bouwer, G. Rottman, and O. R. White (2000), The SOLAR2000 empirical solar irradiance model and forecast tool, *J. Atmos. Sol. Terr. Phys.*, *62*, 1233–1250.

Torr, M. R., D. G. Torr, R. A. Ong, and H. E. Hinteregger (1979), Ionization frequencies for major thermospheric constituents as a function of solar cycle 21, *Geophys. Res. Lett.*, *6*, 771–774.

Wilson, R. J., and K. Hamilton (1996), Comprehensive model simulations of thermal tides in the Martian atmosphere, *J. Atmos. Sci.*, *53*, 1290–1326.

Yoshino, K., A. S.-C. Cheung, J. R. Esmond, W. H. Parkinson, D. E. Freeman, S. L. Guberman, A. Jenouvrier, B. Coquart, and M. F. Merienne (1988), Improved absorption cross-sections of oxygen in the wavelength region 205.240 nm of the Herzberg continuum, *Planet. Space Sci.*, *36*, 1469–1475.

Yoshino, K., J. R. Esmond, A. S.-C. Cheung, D. E. Freeman, and W. H. Parkinson (1992), High resolution absorption cross sections in the transmission window region of the Schumann-Runge bands and Herzberg continuum of O_2, *Planet. Space Sci.*, *40*, 185–192.

Yoshino, K., J. R. Esmond, Y. Sun, W. H. Parkinson, K. Ito, and T. Matsui (1996), Absorption cross section measurements of carbon dioxide in the wavelength region 118.7–175.5 nm and the temperature dependence, *J. Quant. Spectrosc. Radiat. Trans.*, *55*, 53–60.

Yung, Y. L., and W. B. DeMore (1999), *Photochemistry of Planetary Atmospheres*, Oxford Univ. Press, New York.

Zhao, X., and R. P. Turco (1997), Photodissociation parameterization for stratospheric photochemical modeling, *J. Geophys. Res.*, *102*, 9447–9459.

F. González-Galindo and M. A. López-Valverde, Departamento Sistema Solar, Instituto de Astrofísica de Andalucía, Camino Bajo de Huétor 50, Granada 18080, Spain. (ggalindo@iaa.es)

M. Angelats i Coll, Department of Earth and Space Sciences, University of California, Los Angeles, CA, USA.

F. Forget, Laboratoire de Météorologie Dynamique, CNRS, Paris, France.